

STRUCTURAL AND ELECTRICAL CHARACTERIZATION OF LANTHANUM DOPED STRONTIUM HEXAFERRITES

Muhammad Azim, Shahid Atiq and Shahzad Naseem

Centre of Excellence in Solid State Physics, University of the Punjab, Lahore-54590, Pakistan

Author's mailing address: azimnadeem@gmail.com (+923234893009)

ABSTRACT: Sol-gel auto-combustion route was adopted to synthesize lanthanum doped strontium hexaferrites having composition, $La_xSr_{1-x}Fe_{12}O_{19}$ with $x = 0, 0.1, 0.15, 0.2$. The powder samples were annealed at 800 °C for 2 hours in a muffle furnace. X-ray diffraction was performed for all the samples which confirmed the presence of hexagonal phase in the strontium ferrite compositions. The lattice parameters, crystallite size, crystallite volume and X-ray densities were evaluated from the X-ray diffraction patterns. Dielectric measurements were carried out for all the samples prepared in pellets form to find out the dielectric parameters such as dielectric constant and dielectric loss as function of frequency.

1. INTRODUCTION

The origin of ferromagnetism has remained a huge controversy in oxide based dilute magnetic semiconductors [1]. History of ferrites started, in concern, with the search for the ferromagnetic materials of usually high resistivity. As the eddy current losses in the ferromagnetic materials are inversely proportional to the resistivity, so with the use of ferrites having resistivity value of $10^7 \Omega m$, as compared to $10^{-7} \Omega m$ for iron, eddy current loss can be negligibly minimized even at microwave frequencies [2]. Several methods have been used to synthesize both doped and undoped strontium hexaferrites. For example, solid state method, precipitation techniques [3], solution-evaporation and sono-chemical methods have been used for the formation of ferrites. However, sol-gel auto-combustion method has recently, emerged as a novel technique to prepare such kind of materials in pure phase [4]. A key advantage of this technique is that ceramic oxide materials can be prepared at relatively low temperatures as compared to other techniques which require high temperature treatment and hence, energy consuming and costly. In addition, most of the preparation techniques give rise to the formation of Sr_2O_3 and $Si_2Fe_4O_9$ along with the required phase. To overcome these difficulties, the sol-gel auto-combustion technique is used in the present work.

2. EXPERIMENTAL

La-doped strontium ferrite samples were prepared having a general formula, $La_xSr_{1-x}Fe_{12}O_{19}$ with $x = 0, 0.1, 0.15$ and 0.2 , using sol-gel auto-combustion technique. Physical and chemical properties of oxide materials synthesized with combustion process mainly depend on the nature and amount of the fuel-agent used. Various organic fuels, for instance, urea, glycine, acetic acid and sucrose are employed in this technique. However citric acid, being low-cost, has been successfully employed, for the preparation of oxide materials [1]. First, stoichiometric molar ratios of the reagents, such as iron nitrate [$Fe(NO_3)_3 \cdot 9H_2O$], lanthanum nitrate [$La(NO_3)_3 \cdot 6H_2O$], strontium nitrate [$Sr(NO_3)_2$] and citric acid, all of analytical grade purity, were dissolved in de-ionized water to form a homogenous solution, having a total volume of 50 ml. In the next step, the homogeneous mixture was placed on a magnetic hot plate to obtain a sol, which converted into a gel, with continuous stirring using a magnetic stirrer at 150°C. The gel was further heated at 300°C until it was burnt vigorously and completely. The end product was a fluffy powder which was grinded using a

mortar and pestle to obtain uniform grain size. The powder samples were annealed at 800 °C for 2 hours in a muffle furnace. X-ray diffraction (XRD) analysis of the powder samples was performed to investigate the crystal structure. An Apex hydraulic press having a steel dye of 13 mm diameter was used to make pellets. The pellets were then used to characterize the dielectric behavior of the samples using an LCR meter.

3. RESULTS AND DISCUSSION

X-rays are exactly of the same nature as light but with much shorter wavelength. The wavelength of X-rays lies in the range of 0.5-2.5 Å. In the electromagnetic spectrum, they are found between the gamma and ultraviolet rays. These radiations have been of a great importance to physics and chemistry of solids in two key features of research, namely in the finger print identification of crystalline materials and in the determination of their structure. XRD is based on the interaction between X-rays of a particular wavelength and the atomic rows in a crystalline material. X-rays are diffracted by lattice planes at specific angles that are characteristics of each individual type of inter-planer spacing, as shown in Figure 1. The angles depend on inter atomic spacing and the wavelength of the incident X-rays according to Bragg's law:

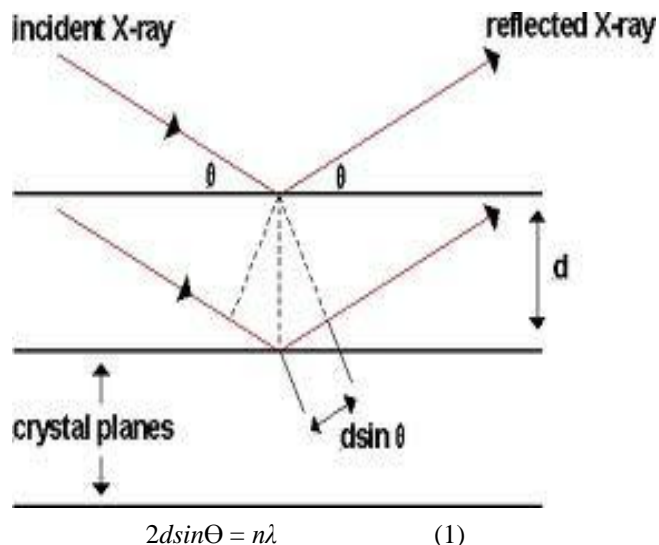


Figure 1 Bragg's diffraction condition

Where ‘n’ is an integer, ‘d’ is the lattice spacing and ‘θ’ is the diffracting angle. The diffraction patterns of all the prepared samples are shown in Figure 2. For indexing the pattern, the role of structure factor in the hexagonal ferrite structure, is first determined from the resultant wave, scattered by all the atoms of the unit cell. It explains the arrangements of atoms in the crystal structure. If a unit cell contains 1,2,3, …..N atoms with fractional coordinates $u_1v_1w_1, u_2v_2w_2, u_3v_3w_3, \dots$, and f_1, f_2, f_3, \dots are the atomic scattering factors, then the structure factor for the (hkl) reflections is given by Eq.2 [5],

$$F_{hkl} = \sum_{i=1}^N f_i e^{2\pi i(hu + kv + hw)} \quad (2)$$

Where ‘F’ is a complex number which represents the amplitude as well as the resultant wave vector. The following are the allowed values of (hkl) which can appear in the hexagonal structure according to structure factor calculations shown in Table 1 [5].

Table1 Allowed values of hkl in hexagonal structure

h+2k	L	F ²
3m	Odd	0
3m	Even	4f ²
3m±1	Odd	3f ²
3m±1	Even	f ²

The constraints mentioned in Table 1 help us to solve the XRD pattern. Problems may arise, there are some unknown diffraction lines present due to impurities in material or due to any other reasons, which needs extra skills to solve them. For solving and indexing the pattern, a relation is developed by combining plane-spacing equation and Bragg law’s equation which determines the Miller indices of some specific crystal system, as described in Eq. 3,

$$\sin^2\theta = A(h^2+hk+k^2) + C \quad (3)$$

Where, $A = \lambda^2/3a^2$ and $C = \lambda^2/4c^2$ are constants, ‘a’ and ‘c’ are the lattice parameters which were calculated after solving the XRD pattern. Following the complete procedure and calculations [5], the diffraction patterns were indexed as shown in the Figure 2. All the indexed peaks were characteristics of the SrFe₁₂O₁₉ with hexagonal structure. No impurity peaks related to any other oxides, e.g. Fe₂O₃ and La₂O₃ were observed in the present case, as were observed in the work already reported for x =0.2 [6].

For any close packed hexagonal system, lattice parameters can be determined by solving equation 3 for various values of sin²θ [5]. The lattice constants ‘a’ and ‘c’ were evaluated for all the samples of the series, La_xSr_{1-x}Fe₁₂O₁₉ with x = 0, 0.1, 0.15 and 0.2. The variation in both the lattice constants with increasing ‘x’ is shown in Figure 3. It has been observed that both the lattice constants ‘a’ and ‘c’ increase slightly with the increasing concentration of lanthanum at the strontium sites. This trend may be attributed to the substitution of lanthanum having larger ionic radii as compared to the strontium, which is being replaced [7-8]. The crystallite size was determined using the most intense peaks present in the diffraction pattern. The calculations

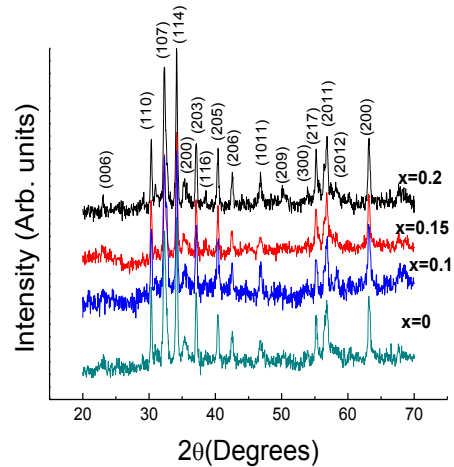


Figure 2: XRD patterns of La_xSr_{1-x}Fe₁₂O₁₉

were preceded using Scherrer’s formula [9], as given below, $D = k\lambda / (B \cos\theta)$ (4)

where ‘D’ is the crystallite size, ‘k’ is the constant which has a value of 0.94, ‘λ’ is the wavelength of Cu-Kα source used in X-ray diffraction, ‘B’ is the full width at half maxima in radians and ‘θ’ is the diffraction angle. Utilizing this relation, the crystallite size was determined which showed an increasing trend in the range of 29.86-34.576 nm for all the samples. This is due to the fact that in the material lanthanum ions are continuously being substituted at the strontium sites [8]. The bulk density of the material was determined by using the relation, $\rho_b = m / \pi r^2 h$, where ‘ρ_b’ is the bulk density of the material, ‘m’ is the mass of the pellet in grams, ‘r’ is the radius of the pellet in cm, ‘h’ is the thickness of the pellet in cm. The bulk density measured for all the compositions showed an increasing trend ranging from 3.19 to 4.51 g/cm³.

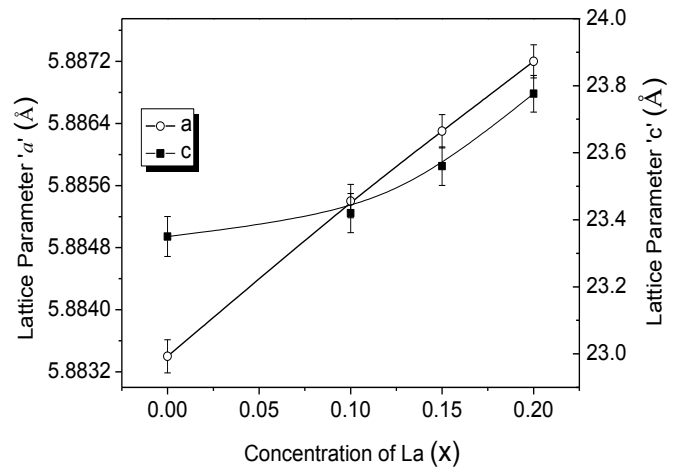


Figure 3: Variation of lattice parameters with composition ‘x’

Table 2 Calculated values of lattice parameters ‘a’ and ‘c’, c/a ratio, volume of the cell (V), crystallite size (D), bulk density of the material (ρ_b), X-ray density (ρ_x) and porosity

Parameter	x =0.00	x =0.1	x =0.15	x =0.2
a(Å)	5.8834	5.8854	5.8863	5.8872
c(Å)	23.35	23.42	23.56	23.776
c/a	3.9687	3.9793	4.0025	4.0385
V(Å) ³	699.941	702.516	706.933	713.63
D(nm)	29.86	31.654	33.483	34.576
ρ_b (g/cm ³)	3.19	3.71	4.51	3.72
ρ_x (g/cm ³)	5.28	5.045	5.025	4.991
Porosity(%)	39.5	26.4	10.2	25.4

X-ray density was determined with the help of the relation, $\rho_x = 2M/N_A V$. Here ‘M’ is the molecular weight of the material, ‘N_A’ is the Avogadro's number and ‘V’ is the volume of the unit cell. X-ray density also had an increasing trend ranging between 4.97-5.18 g/cm³ due to the increasing concentration of lanthanum in the material [8]. This increasing trend in X-ray densities and in bulk density decreases the porosity of the samples.

The electric response of a dielectric can be described by its dielectric constant and dielectric loss factor. In order to investigate the dielectric properties of La_xSr_{1-x}Fe₁₂O₁₉ (x = 0, 0.1, 0.15, 0.2), the frequency dependent dielectric constant and dielectric loss were determined using a precision 1920 QaudTech LCR meter. The measurements were taken in the frequency range of 100 Hz to 1 MHz at room temperature. The samples were used in disk form having a diameter of 13 mm and thickness between 0.6 mm to 1 mm. Values of capacitance and parallel resistance were obtained as a function of frequency for all the samples. The dielectric constant was determined from the relation [10],

$$\epsilon' = \frac{Ct}{\epsilon_0 A} \tag{5}$$

where ‘C’ is the capacitance of the pellet in farad, ‘t’ is the thickness of the pellet in meters, ‘A’ is the cross-sectional area of the flat surface of the pellet and ‘ ϵ_0 ’ is the permittivity of free space. The tangent of dielectric loss angle can be evaluated using the relation given as,

$$\text{Tan}\delta = \frac{1}{2\pi f C_p R_p} \tag{6}$$

Where ‘ δ ’ is the loss angle, ‘f’ is the frequency, ‘R_p’ is the equivalent parallel resistance and ‘C_p’ is the equivalent parallel capacitance. The dielectric loss factor was also measured in terms of tangent loss factor defined by the relation,

$$\epsilon'' = \epsilon' \text{tan}\delta \tag{7}$$

Figure 4 shows the dielectric constant as a function of frequency for all the samples. As can be seen in the figure, the dielectric constant decreases rapidly with the increase in frequency and becomes independent at high frequencies. The decrease in the dielectric constant at low frequencies is mainly due to the dielectric relaxation. The dielectric dispersion can be explained by Koop’s theory. According to this theory, the dielectric structure is considered to consist of double layers, where one layer is conducting and other one is insulating. According to Koop’s structural point of view, dielectric relaxation is directly linked to orientation polarization. On applying external field, atoms of the dielectric material takes some time to align them in the direction of applied electric field and that time is known as relaxation time which is precisely equal to 10⁻⁹ s.

It is observed that the decrement in dielectric constant with increasing frequency is due to the fact that atoms in dielectric material needs a finite time to align up their axis in the applied field direction. As the frequency of the electric field increases, a point is reached when charge carrier of dielectric material do not align with the applied field so polarization cannot reach at its saturation point and do not follow the fluctuation of applied electric field, so the dielectric constant is decreased. When the frequency of the applied field continues to increase, a stage comes when the polarization starts to lag behind the frequency of field reversal. Therefore, dielectric constant becomes independent at very high frequency. Another valid point for the decrement in dielectric constant is related with the hopping of electrons from Fe²⁺ to Fe³⁺ ions which require a specific amount of energy [10]. At low frequencies, electric field does not provide enough energy to electrons. As the frequency of the electric field is increased, it provides sufficient energy and a point is reached when hopping of electrons is started from Fe²⁺ to Fe³⁺. In this case,

$$\omega T = 1 \tag{8}$$

Where ‘T’ is the relaxation time of the hopping process, ‘ ω ’ is the angular frequency. It is obvious that relaxation time is inversely proportional to the jumping probability per unit time, ‘P’, defined as,

$$T = \frac{P}{2} \tag{9}$$

The increase in jumping probability is directly associated with the increase of ferrous ions on B-site, which is responsible for the polarization in these hexagonal ferrites. That is why conductivity of the dielectric increases as frequency is increased and decrement occurs in dielectric constant.

When the relaxation time of dielectric material and the frequency of the applied field become similar, a phase lag occurs and energy observed in dielectric material, is called dielectric loss.

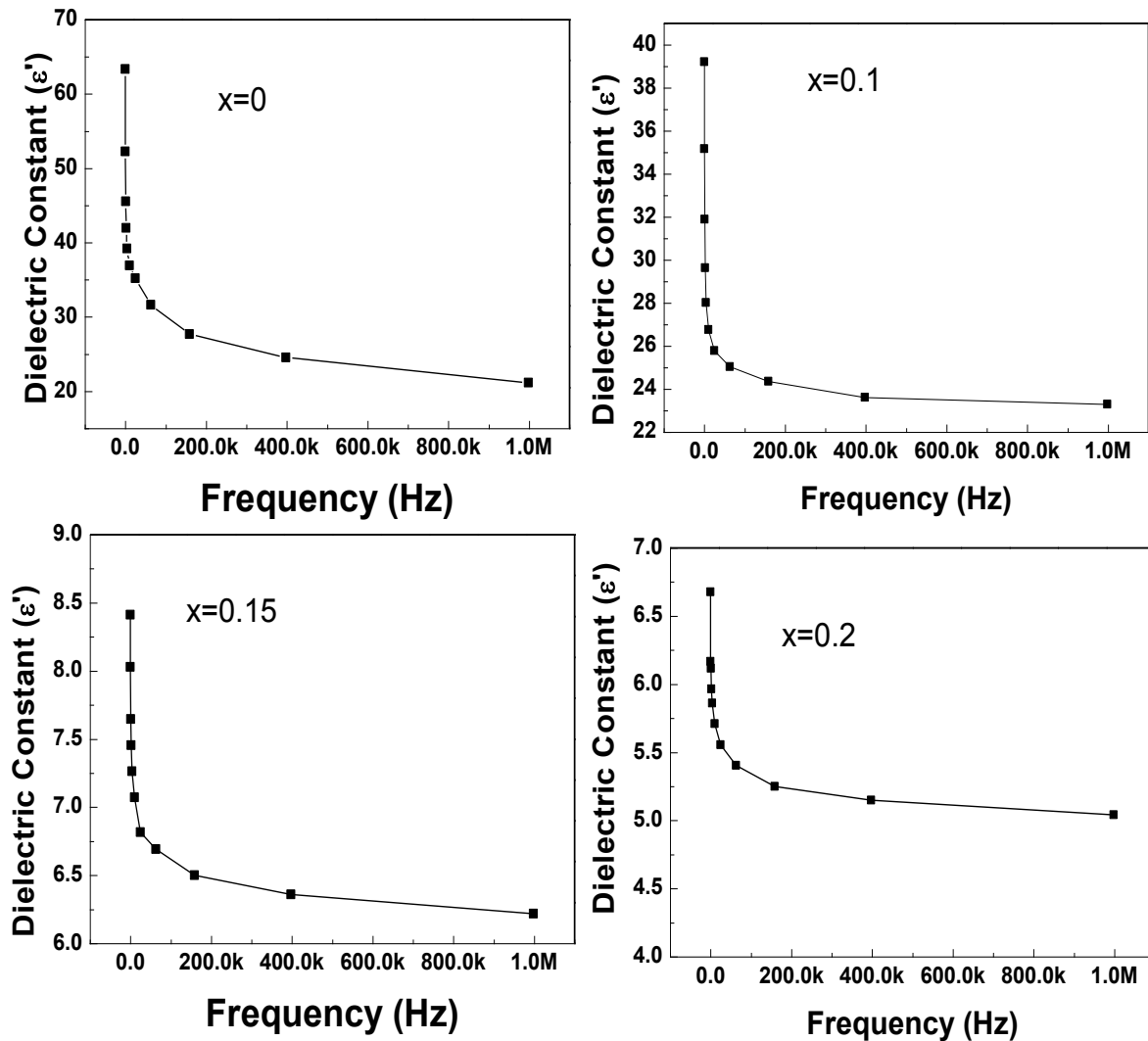


Figure4: Dependence of dielectric constant on frequency for $\text{La}_x\text{Sr}_{1-x}\text{Fe}_{12}\text{O}_{19}$ samples

It is observed that dielectric loss ϵ'' is greater in the case of La-substituted strontium hexa-ferrites. The trend of dielectric loss is decreasing as the concentration of dielectric loss is gradually decreased with an increase in 'x'. These losses in hexagonal ferrites are basically reflected in the resistivity and conductivity measurements. It has been reported repeatedly that the materials which possess high value of resistivity and low value of conductivity exhibit low dielectric loss and vice versa [9]. An increase in the dielectric loss value in La^{3+} substituted Sr-hexaferrites confirms the increase in conductivity, which is in accordance with the Verway's conduction mechanism [13-14].

4 CONCLUSIONS

Strontium hexagonal ferrites with composition $\text{La}_x\text{Sr}_{1-x}\text{Fe}_{12}\text{O}_{19}$ ($x = 0, 0.1, 0.15, 0.2$) were prepared by sol-gel auto-combustion method. The prepared samples were annealed at 800 °C for two hours. X-ray diffraction analysis confirmed the existence of hexagonal phase in all the four samples. Lattice parameters of the crystal system were also

determined from the data obtained from the diffraction pattern. It has been observed that the lattice constants ' a ' and ' c ' increases slightly. This may be attributed to the substitution of lanthanum at strontium sites. Crystallite size was determined in the range of 29.86-34.576 nm, with an increasing trend. Bulk density of the materials showed an increasing trend, whereas, x-ray slightly decreases which causes porosity slightly decreased in the series. It has been noticed that dielectric constant decreases sharply with the increase in frequency and finally becomes independent at high frequencies. This decrease in the dielectric constant is mainly due to the dielectric relaxation, which is in accordance with the Koop's theory. The trend of dielectric loss is also decreasing because with the addition of La^{3+} at Sr^{2+} sites, it is observed that dielectric loss gradually decreases which is in good agreement with the Verway's conduction mechanism.

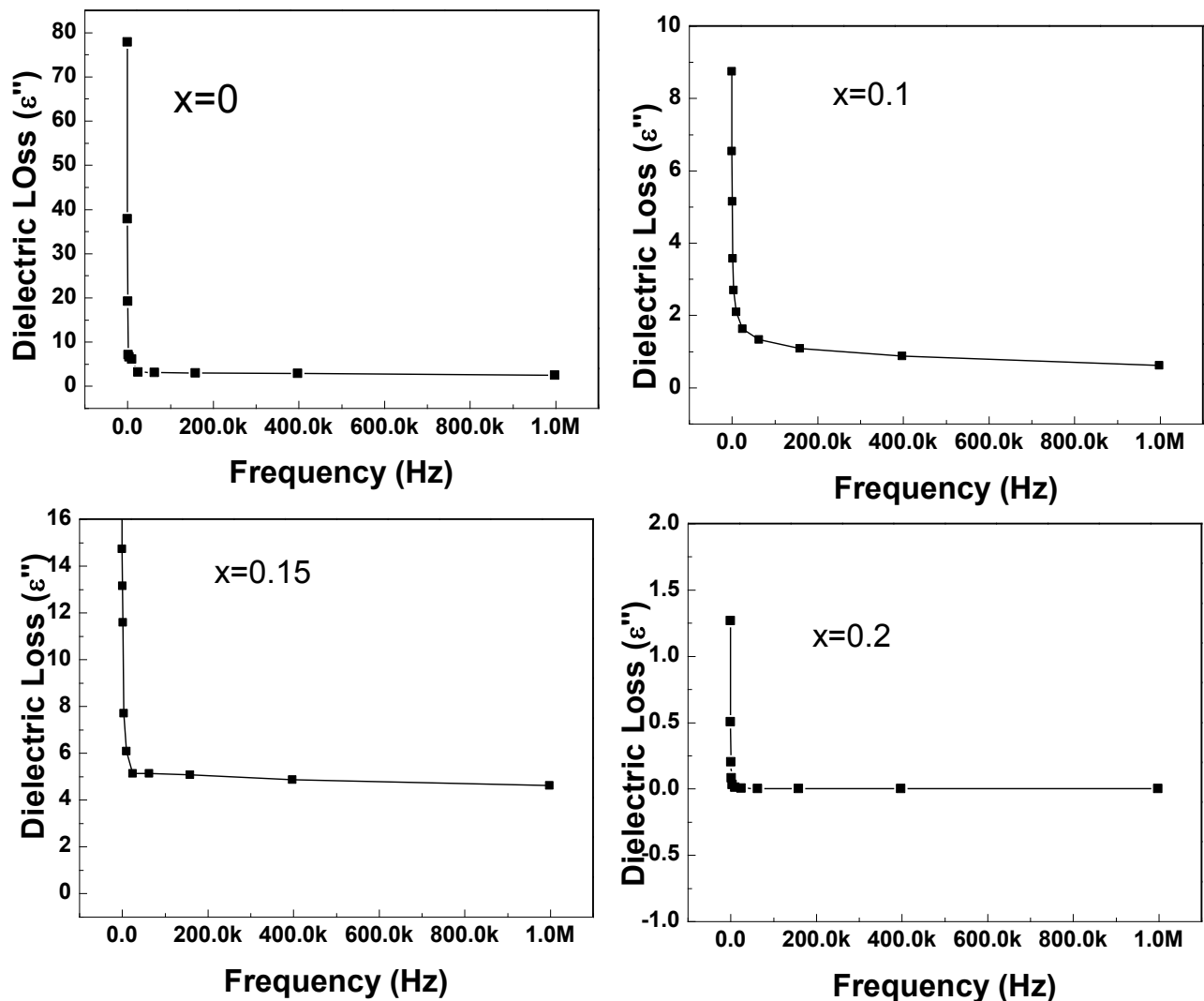


Figure 5: Dependence of dielectric loss on frequency for $\text{La}_x\text{Sr}_{1-x}\text{Fe}_{12}\text{O}_{19}$ samples

REFERENCES

- [1] M. Saleem, S.A. Siddiqi, S. Atiq, S. Anwar, I. Hussain, and S. Alam, *Mater. Charac.*, **62**, 1102-1107 (2011).
- [2] J. Qui, R. Gong, Z. Feng, and J. Liao, *Mater. Sci. Eng. B* **170**, 155-158 (2010).
- [3] A. Drmota, M. Drogenik, and A. Znidarsic, *Ceram. Inter.*, **38**, 973-979 (2012).
- [4] R. M. Garcia, V. Bilovol, and L.M. Socolovsky, *Physica B*, **407**, 3109-3112 (2012).
- [5] B. D. Culity, *Elements of X-ray Diffraction*, 2nd Ed., Addison-Wesley Publishing Company, Inc., 1978.
- [6] X. Liu, W. Zhong, S. Yaug, Z. Yu, B. Gu, and Y. Du, *J. Magn. Magn. Mater.*, **238**, 207-214 (2002).
- [7] S. Ounnukad, *Solid State Commun.*, **138**, 472-475 (2006).
- [8] W. Onreabaroy, K. Papato, G. Rujjanagul, K. Pengpat, and T. Tunkasiri, *Ceram. Inter.*, **38**, S415-S419 (2012).
- [9] S. C. Watawe, B. D. Sarwade, S. S. Bellad, B. D. Sutar, and B. K. Chaougule, *J. Magn. Magn. Mater.*, **214**, 55-60 (2000).
- [10] M. N. Ashiq, M. J. Iqbal, and I. H. Gul, *J. Alloys Compds.*, **487**, 341-345 (2009).
- [11] D. R. Ravinder, P. Vijaya, and B. Reddy, *Mater. Lett.*, **57**, 4344-4350 (2003).
- [12] A. M. Shaikh, S. S. Belled, and B. K. Chougule, *J. Magn. Magn. Mater.*, **195**, 384-390 (1999).
- [13] N. J. Ali, J. Rahman, and M. A. Showdhury, *Jpn. J. Appl. Phys.*, **39**, 3378-3381 (2000).
- [14] A. Y. Lipare, P. N. Vasambekar, and A. S. Vaingaskar, *Phys. Stat. Solidi A*, **196**, 372-378 (2003).